CIMAC CONGRESS 25
ZURICH, MAY 19 – 23, 2025

2025 | 159

Investigation on the thermal cavitation effect of an injector control valve

Fuel Injection & Gas Admission and Engine Components

Jianhui Zhao, Harbin Engineering University

Weilong Liu, Harbin Engineering University
Xiang Tan, Harbin Engineering University
Yu Xu, Harbin Engineering University

DOI: https://doi.org/10.5281/zenodo.15236736

ABSTRACT

Cavitation occurs readily within the control valve of a common rail injector, significantly impacting the response characteristics and injection performance of the injector, which in turn affects the dynamic and economic performance of diesel engines. In this study, a mathematical mapping between turbulent viscosity and temperature gradient was constructed, and a modified turbulence model incorporating transient turbulent viscosity was proposed. Using this modified model, a simulation study on the thermal cavitation characteristics of fuel within the control valve was conducted. The results indicate that substantial cavitation occurs along the ball valve and valve seat walls during fuel flow within the control valve. The intense cavitation region on the ball valve surface is located behind the sealing surface of the control valve, where the unique geometric structure causes fuel flow separation, subsequently leading to vortex formation and cavitation. The mainstream flow bypasses this region, making it difficult for the cavitation to be expelled. Cavitation on the valve seat wall arises due to a sudden reduction in flow area and an abrupt change in flow direction at the inlet, causing a sharp pressure drop. Additionally, this cavitation is influenced by the cavitating flow within the guide hole. The fuel within the control valve is more significantly affected by viscous heating than by the latent heat of phase change, resulting in an increase in fuel temperature. The temperature rise distribution of fuel within the control valve is highly consistent with the distribution of cavitation, with significant temperature rises occurring in the cavitation core areas at the ball valve and valve seat walls. The peak temperature reaches 460 K, and the maximum average temperature rise at the valve seat wall is 57.79%. The heat from the high-temperature fuel at the walls is conducted to the flow's central area through vortex structures, creating a noticeable temperature gradient from the control valve wall to the central flow area, with both temperature rise and gradient increasing with inlet pressure.

1 INTRODUCTION

Diesel engines are renowned for their high energy conversion efficiency, strong power, and ease of maintenance, making them the primary power source for ships and commercial vehicles. In the context of energy conservation and emission reduction, the development of diesel engines toward higher efficiency, cleanliness, and power density is inevitable. The high-pressure common rail (HPCR) system is an effective means to enhance engine performance.

In current, the injection pressures of commercial HPCR range from 160 to 180 MPa. Under such high pressure, cavitation is highly likely to occur within the injector, particularly in the nozzle and control valve. Previous research has investigated cavitation flow characteristics within injector nozzles, with analyses focusing on the effects of nozzle structure [1-3], ambient pressure [4], fuel properties [5, 6] on cavitation flow. Studies have also explored the causes of cavitation through vorticity [7] and temperature distribution [8], yielding significant findings.

Cavitation in the control valve of an injector is a key factor affecting flow performance, which in turn influences the response characteristics of the fuel injector. Some researchers have conducted experimental studies on cavitation flow within control valves using visualization methods. Karathanassis et al. [9] and Chen et al. [10] utilized X-ray to capture the cavitation distribution within control valves, though this requires high-frequency X-ray equipment and is costly. Ma et al. [11] conducted a two-dimensional visualization experiment, discovering that the cavitation occurred at the surface of seal cone and steel ball, and the cavitation collapse area was at the downstream of the seal annulus. Liu et al. [12] employed a three-dimensional visualization experiment to study cavitation in the injector control valve. It was found that the cavitation locations coincide with the damage sites observed in the ball seat, which proves that cavitation damage is the main factor causing seal failure in ball valves. Sun et al. [13] developed a multi-view visualization equipment, combined with feature recognition technology, significantly enhancing the visualization of cavitation flow within control valves. Despite the ability of visualization experiments to directly observe cavitation, limitations in the strength and sealing of transparent materials restrict experiments to lower pressures, differing from actual cavitation within control valves. Moreover, the brief duration from the initial opening to full opening of the control valve, occurring in milliseconds or microseconds, makes it challenging for high-speed cameras to capture subtle change during cavitation process.

With advances in computer performance and numerical model theories, more researchers are utilizing numerical computation methods to study the cavitation. Some scholars have focused on the impact of cavitation on flow characteristics to reveal its role in the performance of control valves. Ren et al. [14] found that cavitation led to a slower response of the control valve but had a remarkable effect on reducing the hydraulic shock to the ball valve and sealing cone, as well as stabilizing the fluctuation of fuel velocity in the control chamber. Bianchi et al. [15] investigated the effect of cavitation on the discharge coefficient of OA hole at different pressure differences and found that the discharge coefficient varies with pressure difference due to the variation of the cavitation number and the contraction coefficient at the maximum ball valve lift. Wang et al. [16] studied cavitation flow within control valves under different structural parameters, showing that the mass flow rate increases continuously with the increase of the section area, and cavitation within the control valve impedes the increase of the mass flow rate. Additionally, some scholars focus on factors influencing cavitation, aiming to suppress it within control valves. Kayakol et al. [17] found that the stagnation flow effect resulting from the deceleration of the flow in front of the ball valve, as well as the separation and reattachment of fuel flow along the surface, had a significant impact on the development of cavitation in the ball valve. Zhao et al. [18] investigated the cavitation within the control valve and found that there are differences in the distribution of cavitation regions occurring on the ball and ball seat. The stagnation effect caused by the ball exacerbates the discrepancy in the distribution of the intense cavitation region between the ball and the ball seat. Miao et al. [19] revealed that cavitation mainly occurs around the sealing surface, with its formation and development depending on the ball valve lift and nearby fuel pressure, worsening with increased lift. Ko et al. [20] identified the throttle area and inlet area of the ball valve as the main structural factors influencing cavitation, and proposed an optimization design method to minimize cavitation.

The majority of the aforementioned simulation studies were conducted under the assumption that the fuel was isothermal and incompressible. However, as HPCR systems evolve toward ultra-high pressures, the flow within the injector experiences larger pressure differences and higher flow velocities. This results in significant frictional heating within the control valve, leading to a non-isothermal fuel flow. Additionally, this frictional heating causes uneven temperature distribution, which in turn affects cavitation distribution. Previous research has focused on the effects of cavitation and methods to mitigate it. Although

some scholars have analyzed the characteristics of cavitation distribution within the control valve, there is still a lack of in-depth research on the cavitation mechanisms and the coupled relationship between cavitation distribution and temperature distribution. Therefore, in this paper, a non-isothermal compressible flow model for the fuel within the control valve was proposed. The mechanisms of cavitation formation and its coupling relationship with thermal characteristics were revealed.

2 NUMERICAL METHODS

2.1 Governing equations

In this study, two-phase flow simulations were conducted using ANSYS Fluent, employing a Eulerian multiphase model. In this framework, both phases share the same velocity, pressure, and temperature. The mass, momentum, and energy conservation equations are solved for the mixture phase. The mass conservation equation is as follows:

$$\frac{\partial \rho_{\mathrm{m}}}{\partial t}+\nabla\cdot\left(\rho_{\mathrm{m}}U\right)=0 \tag{1}$$

where, ρ_{m} is the mixture density, t is the time, U is the average velocity of mass microelement.

The momentum conservation equation is as follows:

$$\begin{aligned}&\frac{\partial\left(\rho_{\mathrm{m}}U\right)}{\partial t}+\nabla\cdot\left(\rho_{\mathrm{m}}UU\right)=-\nabla\cdot p+\nabla\cdot\left[\mu_{\mathrm{m}}\left(\nabla U+\nabla U^{T}\right)\right]\\&+\rho_{\mathrm{m}}g+F-\nabla\cdot\left(\sum_{\mathrm{k}=1}^{n}\alpha_{\mathrm{k}}\rho_{\mathrm{k}}U_{\mathrm{dr,k}}U_{\mathrm{dr,k}}\right)\end{aligned} \tag{2}$$

where, p is the pressure, μ_{m} is the mixture viscosity, g is the gravitational acceleration, F is the body force, α_{k}, ρ_{k}, $U_{\mathrm{dr,k}}$ are the volume fraction, density and slip velocity of k phase, respectively.

The energy conservation equation is as follows:

$$\begin{aligned}&\frac{\partial}{\partial t}\sum_{\mathrm{k}}\left(\partial_{\mathrm{k}}\rho_{\mathrm{k}}E_{\mathrm{k}}\right)+\nabla\cdot\sum_{\mathrm{k}}\left(\partial_{\mathrm{k}}U_{\mathrm{k}}\left(\rho_{\mathrm{k}}E_{\mathrm{k}}+\rho\right)\right)\\&=\nabla\cdot\left(k_{\mathrm{eff}}\ \nabla T-\sum_{\mathrm{k}}\sum_{j}h_{\mathrm{j,k}}J_{\mathrm{j,k}}+\left(\tau_{\mathrm{eff}}\ \cdot U\right)\right)+S_{\mathrm{h}}\end{aligned} \tag{3}$$

where, E_{k} is the total energy of k phase, k_{eff} is the thermal conductivity, $h_{\mathrm{j,k}}$ is the enthalpy of species j in k phase, $J_{\mathrm{j,k}}$ is the diffusive flux of species j in k phase, S_{h} is the energy source term.

2.2 Fluid properties

During the operation of the injector, due to the extremely high injection pressure and the frictional heating during fuel flow, the fuel properties undergo significant changes with variations in pressure and temperature. In this paper, formulas for key fuel properties, including density, viscosity, and sound speed, were developed using empirical data from the ISO4113 standard test oil [21]. These formulas were integrated into ANSYS Fluent via a user-defined function (UDF) to account for fuel compressibility. The formula for fuel density ρ is as follows:

$$\rho\left(P,T\right)=\frac{a_1+a_2P+a_3P^2+a_4T+a_5T^2}{1+a_6P+a_7P^2+a_8T} \tag{4}$$

where, a_1=834.1684, a_2=3.121, a_3=-6.6×10^{-3}, a_4=-1.8461, a_5=9×10^{-4}, a_6=3×10^{-3}, a_7=-7.3434×10^{-6}, a_8=-1.4×10^{-3}.

The formula for fuel viscosity μ is:

$$\mu\left(P,T\right)=\frac{b_1+b_2P+b_3P^2+b_4T+b_5T^2}{1+b_6P+b_7T+b_8T^2} \tag{5}$$

where, b_1=4.5861, b_2=0.0358, b_3=3×10^{-4}, b_4=-0.0468, b_5=6×10^{-4}, b_6=-3.2×10^{-3}, b_7=-1.6×10^{-3}, b_8=5×10^{-4}.

The formula for fuel sound speed α is:

$$\alpha\left(P,T\right)=\frac{c_1+c_2P+c_3P^2+c_4T+c_5T^2}{1+c_6P+c_7P^2+c_8T} \tag{6}$$

where, c_1=1431.0926, c_2=9.7856, c_3=-0.0189, c_4=3.1×10^{-3}, c_5=-9.0899×10^{-6}, c_6=-5.1049, c_7=-6×10^{-3}, c_8=-9×10^{-4}.

2.3 Correction of the turbulence model

The primary turbulence numerical methods encompass the direct numerical simulation (DNS), large eddy simulation (LES), and Reynolds-averaged Navier-Stokes (RANS) model. DNS directly solves vortices of all scales, posing challenges in predicting intricate turbulence within finite computational constraints. LES tackles large-scale vortices directly and employs turbulent models to characterize small-scale vortices. While this approach mitigates computational complexity, applying it to practical engineering issues remains challenging. RANS resolves vortices entirely through modeling, thereby minimizing computational demands, and currently serves as the principal numerical method in turbulence simulation [22, 23]. In this study, the RANS method was selected for numerical computations.

The k-ε two-equation model within the RANS framework encompasses the standard k-ε model,

the RNG *k-ε* model, and the realizable *k-ε* model, among others. In the injector control valve, frictional heating of the fuel leads to a temperature rise, and the flow process is accompanied by intense transient thermal effects. However, these two-equation turbulence models were developed for room temperature flow, and it has limitations in predicting mixing effects in high temperature flows. To improve the performance of the turbulence model in non-isothermal flow calculations, the *k-ε* two-equation model needs to be appropriately modified. Abdol-Hamid et al. [24] modified the Standard *k-ε* turbulence model to account for thermal effects. The data calculated using the modified model matched the experimental data for fuel pressure and temperature distribution in the orifice under high temperature conditions. Saha et al. [25] found that when simulating fuel cavitation flow in the complex geometry of a fuel injector, both the RNG *k-ε* model and the realizable *k-ε* model demonstrated better accuracy compared to the standard *k-ε* model. Additionally, the realizable *k-ε* model was found to be relatively more time consuming compared to the RNG *k-ε* model. Therefore, in this paper, the RNG *k- ε* model is used to conduct research on cavitation flow in the injector control valve. To account for the influence of thermal effects on the RNG *k-ε* model, a mathematical mapping relationship between the turbulence viscosity coefficient and the temperature gradient is established. A modified RNG *k-ε* turbulence model is proposed, as shown in Eq. (7) to (11):

$$\frac{\partial(\rho k)}{\partial t}+\frac{\partial(\rho k u_i)}{\partial x_i}=\frac{\partial}{\partial x_j}\left[\alpha_k\left(\rho C_\mu^*\frac{k^2}{\varepsilon}+\mu\right)\frac{\partial k}{\partial x_j}\right]+G_k+\rho\varepsilon \tag{7}$$

$$\begin{aligned}&\frac{\partial(\rho\varepsilon)}{\partial t}+\frac{\partial(\rho\varepsilon u_i)}{\partial x_i}=\frac{\partial}{\partial x_j}\left[\alpha_\varepsilon\left(\rho C_\mu^*\frac{k^2}{\varepsilon}+\mu\right)\frac{\partial\varepsilon}{\partial x_j}\right]\\&+\frac{C_{1\varepsilon}{}^*\varepsilon}{k}G_k-C_{2\varepsilon}\rho\frac{\varepsilon^2}{k}\end{aligned} \tag{8}$$

where, ρ is the fluid density, t is the time, u_i is the averaged velocity of fluid, μ is the dynamic viscosity, x_i and x_j is the coordinate directions, α_k and α_ε are the turbulent Prandtl numbers of the k and ε equations, respectively, $\alpha_k = \alpha_\varepsilon = 1.39$, G_k is the generation of turbulent kinetic energy owing to the mean velocity gradients, $C_{2\varepsilon}$ is the model coefficient, the default value is 1.68, $C_{1\varepsilon}$* is a model coefficient [26], C_μ* is the modified turbulence viscosity coefficient. C_μ* is calculated using the following equation:

$$C_\mu^*=C_\mu+\frac{C_\mu\left(\frac{k^{3/2}|\nabla T_t|}{\varepsilon T_t}\right)^3}{0.041+f(M_\tau)} \tag{9}$$

$$f(M_\tau)=\begin{cases}0, M_\tau\le 0.25\\ M_\tau{}^2-0.25^2, M_\tau>0.25\end{cases} \tag{10}$$

$$M_\tau=\frac{\sqrt{2k}}{a} \tag{11}$$

where, C_μ is unmodified turbulent viscosity coefficient, the value is 0.0845, ∇T_t is the total temperature gradient, T_t is the total temperature, a is the local sound speed, M_τ is the turbulent Mach number.

2.4 Correction of the cavitation model

In the realm of cavitation flow computation, researchers proposed the Singhal full cavitation model, Zwart-Gerber-Belamri (ZGB) model, and Schnerr-Sauer (S-S) model [27-30], all rooted in the bubble dynamics Rayleigh-Plesset equation. Compared to the Singhal full model and the ZGB model, the S-S model offers the benefits of fewer empirical coefficients and increased computational stability [31]. In studies concerning the two-phase flow of fuel through fuel injectors, a majority of scholars [8, 22, 32] opted for the S-S model for cavitation simulation. Within the S-S model, when the local pressure P falls below the critical cavitation pressure P_v, cavitation bubbles form, leading to the evaporation of fuel from the liquid phase to the gaseous phase. The evaporation rate R_e is determined using Eq. (12). Conversely, when P exceeds P_v, cavitation bubbles collapse, causing the gaseous fuel to condense back into the liquid phase. The condensation rate R_c is calculated using Eq. (13):

$$R_e=\frac{\rho_v\rho_l}{\rho_m}\alpha_v(1-\alpha_v)\frac{3}{r_B}\sqrt{\frac{2}{3}\frac{P_v-P}{\rho_l}},\quad P\le P_v \tag{12}$$

$$R_c=\frac{\rho_v\rho_l}{\rho_m}\alpha_v(1-\alpha_v)\frac{3}{r_B}\sqrt{\frac{2}{3}\frac{P-P_v}{\rho_l}},\quad P>P_v \tag{13}$$

where, ρ_v, ρ_l, and ρ_m are the densities of the gas, liquid, and mixture, respectively, α_v is the vapor volume fraction, r_B is the bubble radius, P_v is the critical cavitation pressure. P_v is defined as follows:

$$P_v=P_{sat}+\frac{1}{2}C_k\rho k \tag{14}$$

where, P_{sat} is the saturation vapor pressure, C_k is a constant, the valve is 0.39, ρ is the fluid density, k is the turbulent kinetic energy.

The fuel flow inside the control valve is characterized by a larger pressure difference and faster flow velocity, and the cavitation flow is

accompanied by intense thermal effects. However, most scholars [33-36] have conducted cavitation simulations of injectors primarily under isothermal conditions, without considering the temperature dependence of P_{sat} and $1/2C_k\rho k$ in Eq. (14). Therefore, in this paper, the turbulence kinetic energy term $1/2C_k\rho k$ is modified using the density function ρ(P, T) provided in Eq. (4) considering the thermal effects on the turbulence kinetic energy term. Additionally, the formula for P_{sat} varying with transient temperature proposed by Chorążewski et al. [37] is used to modify the constant P_{sat} in Eq. (14), and it is embedded into the S-S cavitation model using UDF.

$$P_{sat} = e^{A-\frac{B}{C+T}} \tag{15}$$

where, T is the local temperature, A, B and C are constants. For ISO4113 standard test oil, A, B and C are 22.87, 5369, and 38, respectively.

2.5 Model verification

The modified model was validated using experimental data on the fuel flow inside injector nozzles measured by Hult et al. [38]. Fig. 1(a) shows the geometric model of the injector nozzle, where the diameters of both nozzle holes are 0.8 mm, and the length-to-diameter ratio is approximately 5. The angles between the bottom and top holes and the injector axis are 58° and 78°, respectively. The computational domain is meshed with a structured grid using Ansys ICEM software, as illustrated in Fig. 1(b). During the meshing process, local refinement was applied at the hole inlet and along the surfaces to better capture the fuel flow characteristics in these regions. After performing a mesh independence analysis, the grid number was determined to be 1.74 million, as shown in Fig. 2.

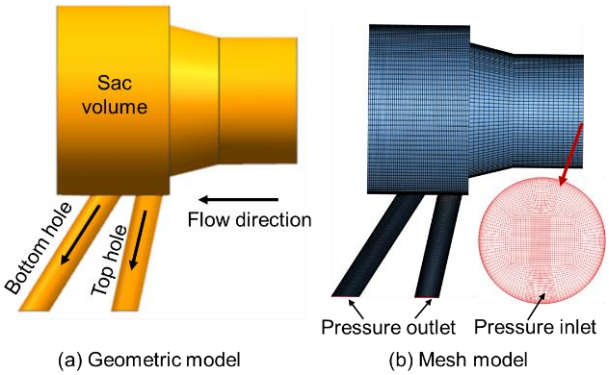

Figure 1. The simulation model of the injector nozzle from Hult's experiment

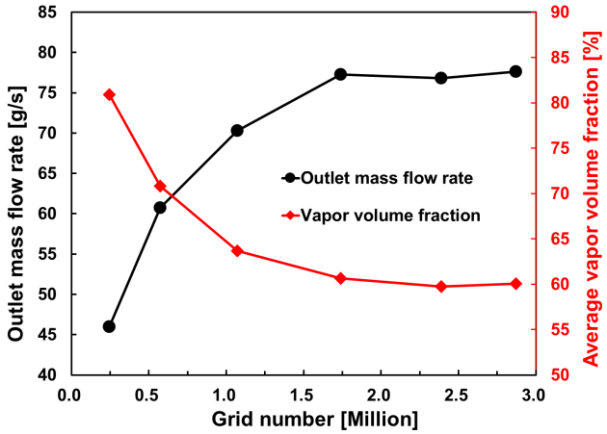

Figure 2. Mass flow rate and vapor volume fraction versus the grid number

The different models were used to simulate the fuel flow within the injector nozzle holes, with the same boundary conditions as those in Hult's experiment. It can be seen from Fig. 3 that, in the simulation results obtained using different models, cavitation in the bottom hole first appears on the left side of the hole inlet and extends along the left surface towards the outlet. For the top hole, cavitation initially occupies the entire hole inlet and then extends towards the outlet, mainly along the left side of the nozzle hole. Moreover, the unmodified model overpredicts cavitation within the nozzle holes, especially in the bottom hole. Overall, compared to the unmodified model, the cavitation distribution obtained from the simulation using the modified model is consistent with the experimental data, demonstrating that the modified model can accurately predict the cavitation distribution.

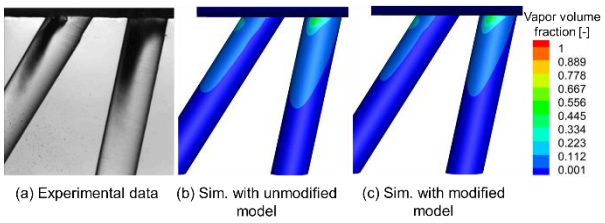

Figure 3. Comparison of calculation results and experimental data [38] for the cavitation distribution (ΔP = 64 bar)

3 MESHING AND BOUNDARY CONDITIONS

The modified turbulence model and modified cavitation model were validated using experimental data. Subsequently, a simulation study on the fuel flow within a self-designed HPCR diesel injector was conducted. The study aimed to analyze the cavitation and thermal characteristics within the injector control valve. Fig. 4(a) presents the simulation domain of the control valve. This model

was constructed based on the actual dimensions of the internal flow path of the injector and includes components such as the control chamber, OZ orifice, OA orifice, guide hole, ball, and ball seat. The detailed structures of each part are shown in Fig. 4(a). The model of control valve in this paper was meshed following the grid division strategy outlined in Fig. 1. Mesh refinement was applied to the ball-ball seat region and the OA orifice, as shown in Fig. 4(b). After conducting a mesh independence analysis, the total grid number was determined to be 2.68 million, with a minimum grid size of 1 μm. This study was conducted under steady-state conditions with the ball valve lifted to a maximum of 0.08 mm, and the detailed boundary conditions are outlined in Table 1.

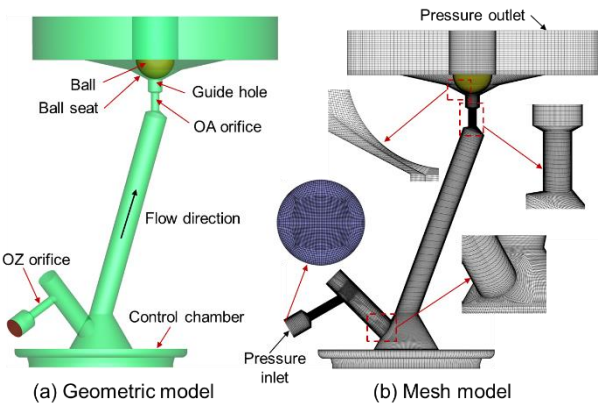

Figure 4. The simulation model of injector control valve

Table 1. Detailed settings of the simulation model

Classification	Setting and/or value
Inlet temperature (K)	345
Inlet pressure (MPa)	160, 200, 250
Outlet pressure (MPa)	0.1
Surface boundary	Adiabatic

The following section will discuss the cavitation flow characteristics within the control valve. The flow domain between the inlet and outlet of the ball valve chamber is the critical area for calculating cavitation flow within the control valve. To analyze the radial distribution of cavitation, four evenly spaced monitoring sections are set between the inlet and outlet of the ball valve chamber. The positions of these monitoring sections are shown in Fig. 5. To quantitatively analyze the cavitation distribution and temperature distribution, monitoring lines are set on the surfaces of the ball and ball seat, as indicated by the blue lines in the figure. These monitoring lines contain several monitoring points, and the vertical height of each monitoring point from the inlet of the ball valve chamber is defined as ΔY.

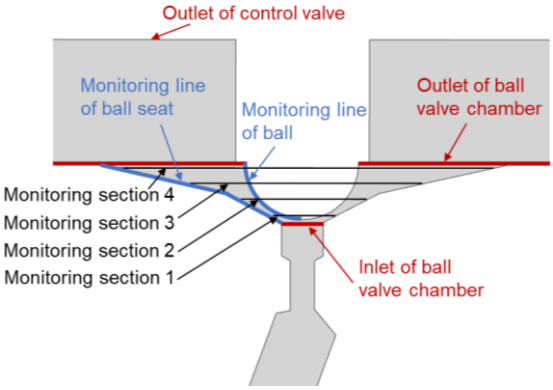

Figure 5. The monitoring lines and sections within the ball valve

4 RESULTS AND DISCUSSION

4.1 Cavitation distribution characteristics in the control valve

Fig. 6 illustrates the axial distribution of cavitation within the control valve under different P_{in}. The figure shows that cavitation within the control valve is asymmetrically distributed, with a greater area and intensity of cavitation on the left side compared to the right. This asymmetry is due to the unique flow channel. Cavitation initially occurs only on the left surface of the OA orifice. As the flow progresses into the guide hole, cavitation develops on both the left and right surfaces, but the left side continues to exhibit a larger cavitation area and higher intensity - a trend that becomes even more pronounced within the ball valve chamber. For the ball in the ball valve chamber, cavitation begins shortly after the flow exits the guide hole. The intensity of cavitation increases along the lower surface of the ball, though it does not merge with the cavitation in the guide hole to form a continuous cavitation region; instead, there is a noticeable gap between them. On the ball seat, cavitation originating from the guide hole progresses along the seat into the ball valve chamber. Cavitation on the ball seat begins closer to the guide hole than on the ball valve. However, the intense cavitation region on the ball seat starts further downstream compared to that on the ball valve. As fuel flows from the ball-ball seat region toward the outlet of the ball valve chamber, the intensity of cavitation on the ball seat first increases and then decreases. Additionally, the distribution and intensity of cavitation within the OA orifice and guide hole show little variation as P_{in} increases, indicating that cavitation in these areas has fully developed. However, cavitation within the ball valve chamber becomes more pronounced with increasing P_{in}. This intensification manifests in two ways: first, the cavitation area expands further downstream and laterally, reaching the horizontal surface connected to the secondary cone surface of the ball seat at P_{in} = 250 MPa, as indicated by the red dashed line in the figure. Second, the

intensity of cavitation within the ball valve chamber increases, primarily reflected in the growth of the intense cavitation region.

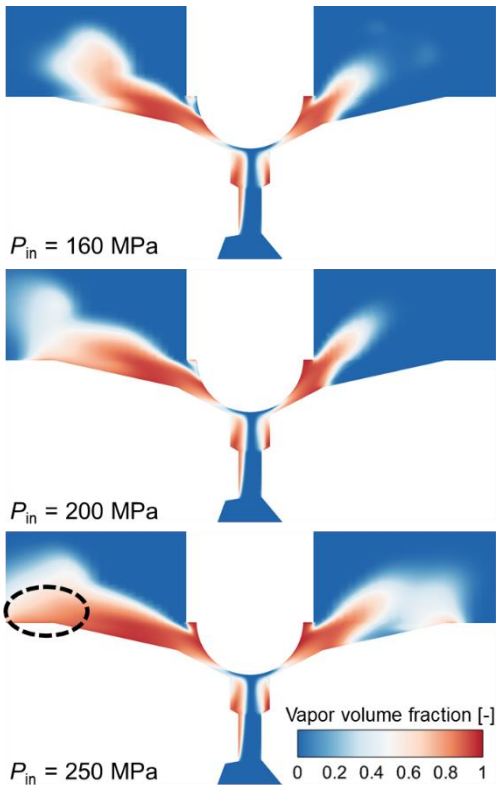

Figure 6. Cavitation distribution along the axial direction of the control valve at different P_{in}

Fig. 7 shows the cavitation distribution on equally spaced sections within the ball valve chamber under different P_{in}. To quantitatively analyze the differences in cavitation distribution, cavitation was categorized based on the vapor volume fraction α_v: cavitation with α_v in the range of 0- 0.3 is defined as slight cavitation, 0.3- 0.8 as medium cavitation, and 0.8- 1.0 as intense cavitation. The area of the cavitation region was quantified using the cavitation area ratio δ, defined as the ratio of the cavitation area to the to the total area of the section.

On Section 1, there is little difference in the area and intensity of cavitation under different P_{in}. When combined with Fig. 8, it is evident that this section primarily exhibits slight and medium cavitation. This is because section 1 is located near the inlet of the ball valve chamber, where cavitation has barely begun on the ball, and the ball seat is just starting to cavitate, resulting in a relatively low level of cavitation development.

On Section 2, the differences in cavitation area and intensity under different P_{in} values remain minimal. However, this region is the cavitation core region, where slight and medium cavitation have progressed to intense cavitation, significantly increasing the area of intense cavitation. The δ for the intense cavitation region at the three P_{in} are 95.1%, 94.6%, and 92.5%, respectively, while the δ for the slight cavitation region decreases to 0.

Section 3 is located at the secondary cone surface, where the flow channel widens. This section is no longer in the cavitation core region, leading to a reduction in the cavitation intensity. At this section, the influence of P_{in} becomes noticeable, with the cavitation distribution expanding as P_{in} increases. The δ for different cavitation intensities also varies with P_{in}. As shown in Fig. 8, the intense cavitation in transitions to slight and medium cavitation. The δ of intense cavitation significantly decreases, with the most substantial reduction occurring under a P_{in} of 200 MPa, where it drops by 32.3%.

On Section 4, the area and intensity of cavitation continue to be influenced by P_{in}. This section is located near the outlet of the ball valve chamber. Compared to section 3, the area of cavitation decreases, and the proportion of the pure liquid region increases. Additionally, the δ for intense cavitation further decreases, with the δ of three P_{in} reducing to 52.1%, 39%, and 57.4%, respectively.

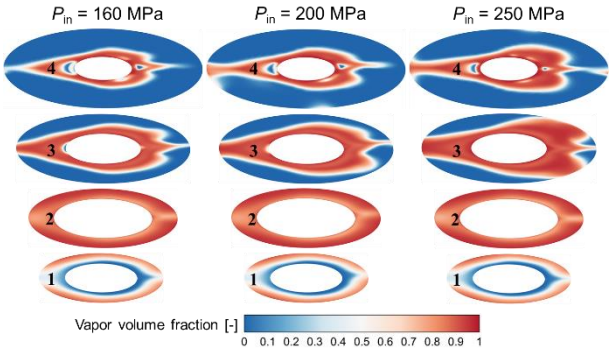

Figure 7. Cavitation distribution along the radial direction of the control valve at different P_{in}

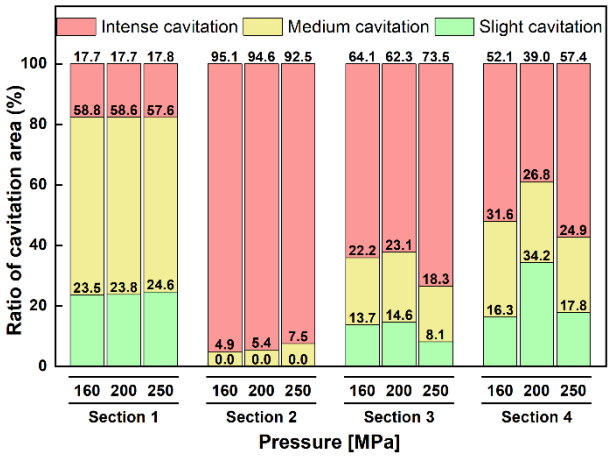

Figure 8. The variation in cavitation intensity of different monitoring sections

4.2 Dynamics analysis of cavitation flow in the control valve

As shown in Fig. 9, the fuel flows through the guide hole and the annular gap between the ball and ball seat, moving towards the outlet of the ball valve chamber. The main flow follows the lower surface of the ball before continuing downstream. The geometric shape of the ball causes the flow passage to expand, increasing the expansion angle. Within the boundary layer, the fuel slows down due to viscous and pressure forces. When its velocity drops to zero, the main flow continues forward, leading to flow separation. The expansion of the boundary layer prevents the fuel within it from moving with the main flow, causing the flow to separate from the ball. The space behind the separation point is filled by recirculating fuel, forming vortices, as indicated by the red dashed lines in the figure. Phase change occurs in the flow separation region, resulting in cavitation near the lower surface of the ball. Additionally, it is observed that at the outlet of the ball valve chamber, a right-angle flow area leads to flow separation and increased vorticity. Cavitation bubbles are drawn into these vortices, accumulating to form a cavitation cloud. As the main flow bypasses this area, the cavitation bubbles are less likely to be carried away by the flow, leading to a persistent cavitated state in this region. This phenomenon is especially pronounced at P_{in} = 250 MPa, where intense cavitation has developed.

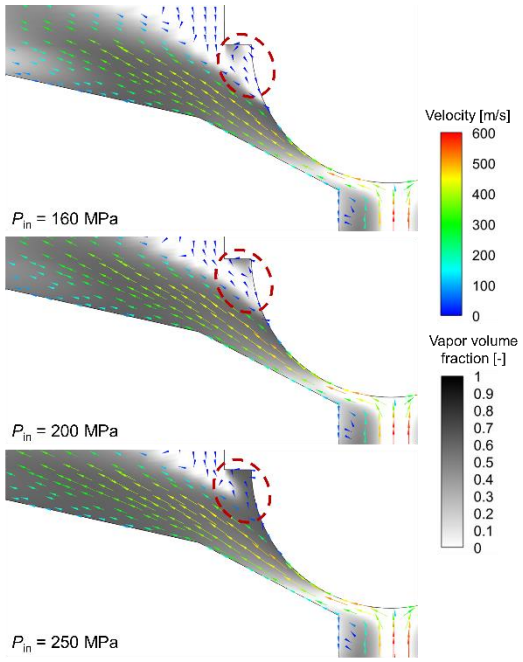

Figure 9. The cavitation and velocity vector within the control valve at different P_{in}

For the ball seat, cavitation first occurs near the outlet of the guide hole and then develops downstream along the ball seat. The cavitation on the ball seat is influenced by the cavitation within the guide hole and eventually merges with it. However, its impact on the cavitation of ball seat is limited due to the cavitation intensity at the guide hole outlet is relatively weak. At the inlet of ball valve chamber, the change in geometry causes a sharp reduction in the flow area and a sudden change in flow direction, leading to intense friction between the high-pressure fuel and the ball seat. Additionally, the local pressure in this region drops sharply according to Bernoulli's equation as the flow velocity increases. Cavitation occurs when the local pressure falls below P_v. Notably, the intense cavitation region on the ball seat is mainly concentrated at the secondary cone surface. As shown in Fig. 10, there is a significant low-pressure region on the ball seat, with the lowest static pressure occurring at the junction between the first and secondary cone surfaces. This creates a substantial pressure drop between the upstream fuel and this region. The free cavitation bubbles on the ball seat, formed due to the reduced static pressure, are carried downstream by the fuel flow and cannot accumulate in this region.

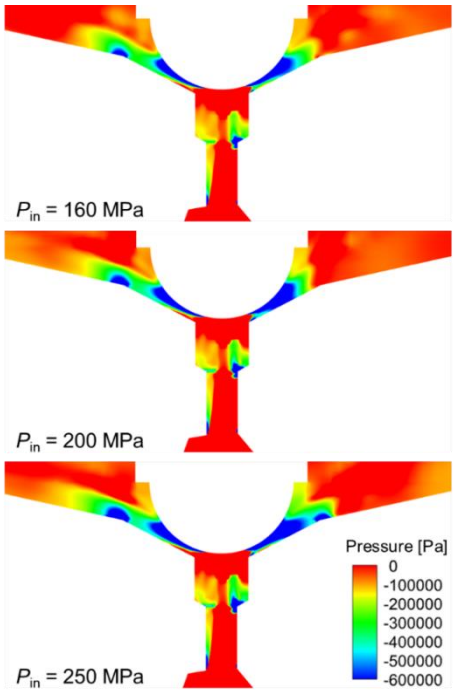

Figure 10. The pressure distribution within the control valve at different P_{in}

4.3 Correlation of thermal and cavitation in the control valve

In this paper, the fuel temperature rise, denoted as ΔT, is introduced to quantitatively analyze the temperature changes induced by thermal effects. ΔT is defined as the difference between the local fuel temperature T and the inlet temperature T_{in}. It

can be seen that the overall temperature within the control valve is on an upward trend, but the ΔT distribution is uneven. T decreases gradually from the control valve surface to the central flow region, creating a noticeable temperature gradient. This gradient is attributed to the viscous heating effect of the fuel, where friction between the fuel and the surface causes the fuel near the surface to heat up. The high-temperature fuel at the surface then transfers heat to the fuel in the central flow region, raising its temperature. Moreover, it is observed that the ΔT distribution corresponds closely to the cavitation distribution. The significant temperature rise regions in the ball valve chamber are located at the cavitation core regions of the ball and ball seat. In the OA orifice, the significant temperature rise region is along the left surface, while in the guide hole, it is along both side surfaces. These patterns align closely with the previously analyzed cavitation distribution within the OA orifice and guide hole. As P_{in} increases, the viscous heating effect becomes more pronounced, leading to higher ΔT and larger temperature gradients. When P_{in} = 160 MPa, the average fuel temperature increases by 2.80%, whereas at P_{in} = 250 MPa, it rises by 4.82%. The ball-ball seat region is identified as the core region for temperature rise within the control valve. The average fuel temperature at the ball and the ball seat increased by 41.98% and 57.79%, respectively.

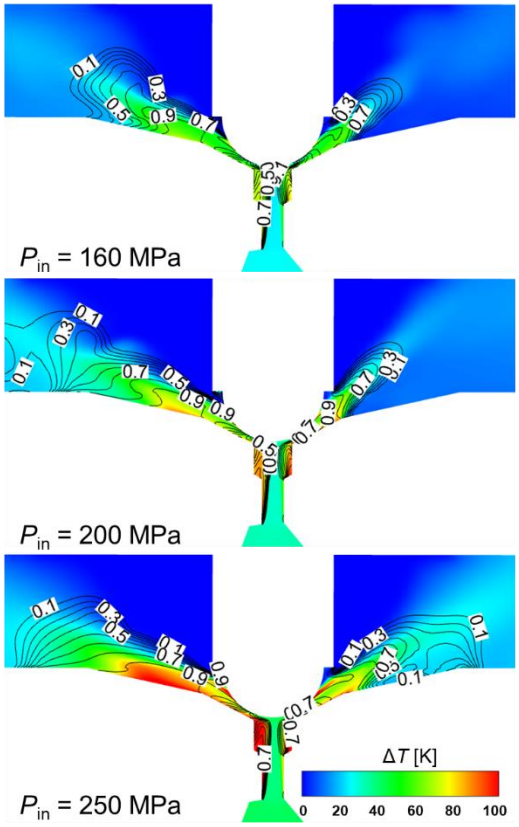

Figure 11. ΔT distribution within the control valve (The black solid lines represent cavitation isoline)

From Fig. 12(a), it can be observed that the vorticity in the central flow region is relatively low, while it increases significantly near the surfaces of the ball and the ball seat. The increased vorticity near the surfaces results in higher shear forces, which intensify the frictional heating of the fuel and cause a rise in fuel temperature at the surfaces. Additionally, the vortex promotes fuel mixing and diffusion, which affects the internal heat transfer, thereby influencing the temperature distribution. Greater vorticity at the surface leads to more pronounced mixing effects of the fuel into the central flow region. During the mixing process, the high-temperature fuel at the surface transfers heat to the central flow region, resulting in an increase in temperature in this region. Moreover, vorticity near the boundary layer induces turbulent flow, leading to a more non-uniform heat transfer process. The thermal effects of the fuel impact the generation and evolution of cavitation in two ways. On the one hand, the fuel density in the core temperature rise region between the ball and ball seat decreases markedly, creating a significant density gradient that induces convection, as shown in Fig. 12(b). These convective effects influence the flow structure and the formation of vorticity. Furthermore, the magnitude and distribution of vorticity affect the occurrence and development of cavitation. Strong vortices promote cavitation because they accelerate fluid movement, causing local static pressure reductions, which promotes cavitation. Vortices can alter the distribution and motion trajectories of cavitation bubbles in the fluid, thereby further affecting the evolution of cavitation. On the other hand, the temperature rise significantly raises the P_v, making cavitation more likely to occur.

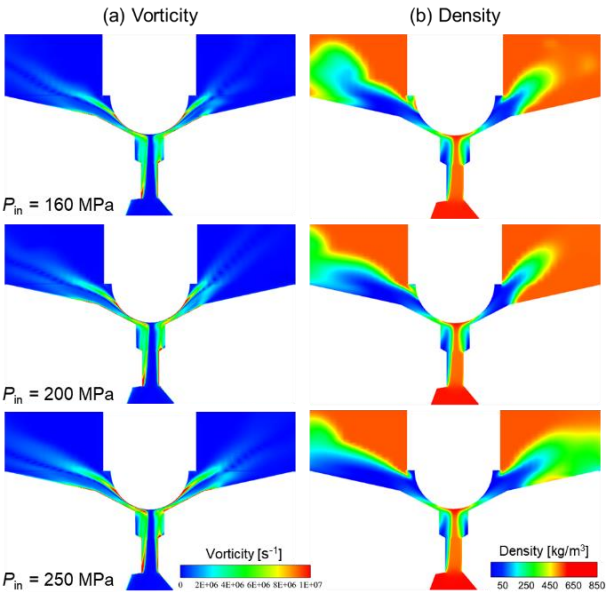

Figure 12. Vorticity and density distribution within the control valve at different P_{in}

5 CONCLUSIONS

In this paper, the turbulence model and cavitation model were modified to account for thermal effects. Numerical simulations were performed using the modified models to investigate the fuel flow characteristics within the control valve. The cavitation distribution characteristics inside the control valve and their coupling relationship with the temperature rise distribution were analyzed. The main conclusions obtained are as follows:

(1) Substantial cavitation occurs along the ball and ball seat walls during fuel flow within the control valve. The intense cavitation region on the ball surface is located behind the sealing surface of the control valve, where the unique geometric structure causes fuel flow separation, subsequently leading to vortex formation and cavitation, The mainstream flow bypasses this region, making it difficult for the cavitation to be expelled. Cavitation on the ball seat wall arises due to a sudden reduction in flow area and an abrupt change in flow direction at the inlet, causing a sharp pressure drop.

(2) There is a significant temperature rise in the fuel within the control valve, with the highest temperature rise occurring at the surface of the ball valve chamber due to more pronounced frictional heating. In regions farther from the surface, frictional heating is less intense, but heat is continuously transferred from the high-temperature fuel at the surface to these regions, leading to a certain degree of temperature rise. Overall, the temperature rise is unevenly distributed. The cavitation also exhibits an uneven distribution, and it overlaps with the region of temperature rise.

(3) The thermal effects within the control valve impact the development of cavitation in two ways. On the one hand, the temperature rise causes a reduction in fuel density, resulting in a significant density gradient between the surface of the ball valve chamber and the central flow region. The strong vorticity generated by the density gradient increases the dynamic pressure of the fluid and decreases the local static pressure, promoting cavitation development. On the other hand, the temperature rise significantly raises the critical cavitation pressure, making cavitation more likely to occur.

6 DEFINITIONS, ACRONYMS, ABBREVIATIONS

P_v: Critical cavitation pressure

P_{sat}: Saturation vapor pressure

P_{in}: Injection pressure

P: Local pressure

ΔP: Pressure difference

ΔT: Temperature rise

α_v: Vapor volume fraction

σ_{cav}: Cavitation volume ratio

δ: Cavitation area ratio

7 ACKNOWLEDGMENTS

This work was supported by the National Key R&D Program of China [grant number 2021YFE0114600].

8 REFERENCES AND BIBLIOGRAPHY

[1] Chen, Z. He, Z. Shang, W. Duan, L. Zhou, H. Guo, G. and Guan, W. 2018. Experimental study on the effect of nozzle geometry on string cavitation in real-size optical diesel nozzles and spray characteristics, *Fuel*, 232: 562-571.

[2] He, Z. Zhou, H. Duan, L. Xu, M. Chen, Z. and Cao, T. 2021. Effects of nozzle geometries and needle lift on steadier string cavitation and larger spray angle in common rail diesel injector, *International Journal of Engine Research*, 22(8): 2673-2688.

[3] Watanabe, H. Nishikori, M. Hayashi, T. Suzuki, M. Kakehashi, N. and Ikemoto, M. 2015. Visualization analysis of relationship between vortex flow and cavitation behavior in diesel nozzle, *International Journal of Engine Research*, 16(1): 5-12.

[4] Prasetya, R. Sou, A. Wada, Y. and Hideaki, Y. 2019. Effects of ambient pressure on cavitation in the nozzle and the discharged liquid jet, *Journal of Fluid Science and Technology*, 14(1): JFST0005.

[5] Aleiferis, P.G. Serras-Pereira, J. Augoye, A. Davies, T.J. Cracknell, R.F. and Richardson, D. 2010. Effect of fuel temperature on in-nozzle cavitation and spray formation of liquid hydrocarbons and alcohols from a real-size optical injector for direct-injection spark-ignition engines, *International Journal of Heat and Mass Transfer*, 53(21-22): 4588-4606.

[6] Bontitsopoulos, S. Hamzehloo, A. Aleiferis, P. and Cracknell, R. 2020. Numerical simulations of the effect of cold fuel temperature on in-nozzle flow and cavitation using a model injector geometry, *SAE Technical Papers*, 2020-01-2116.

[7] Hu, B. He, Z. Li, C. Deng, Y. Guan, W. Zhang, L. and Guo, G. 2024. Study of the effect of cavitation flow patterns in diesel injector nozzles on near-field spray atomization characteristics using a LES-VOF method, *International Journal of Multiphase Flow*, 174: 104791.

[8] Zhao, J. Guo, N. Lu, X. Chen, J. Chen, S. and Zhang, H. 2023. Numerical research on characteristics of fuel heating and subcooling in the nozzle hole of common rail injector, *International Journal of Heat and Mass Transfer*, 200: 123508.

[9] Karathanassis, I.K. Heidari-Koochi, M. Zhang, Q. Hwang, J. Koukouvinis, P. Wang, J. and Gavaises, M. 2021. X-ray phase contrast and absorption imaging for the quantification of transient cavitation in high-speed nozzle flows, *Physics of Fluids*, 33(3): 032102.

[10] Chen, P. Xu, R. Liu, Z. Liu, J. and Zhang, X. 2023. Homogeneous field measurement and simulation study of injector nozzle internal flow and near-field spray, *Processe*, 11(9): 2533.

[11] Ma, H. Zhang, T. An, Q. Tao, Y. and Xu, Y. 2021. Visualization experiment and numerical analysis of cavitation flow characteristics in diesel fuel injector control valve with different structure design, *Journal of Thermal Science*, 30: 76-87.

[12] Liu, J. Liu, Z. Wu, J. Li, Z. Chen, P. and Gu, X. 2022. Visualization experiment and numerical calculation of the cavitation evolution inside the injector ball valve, *Fuel*, 329: 125550.

[13] Sun, F. Xu, H. Meng, Y. and Yin, H. 2023. A novel multi-view enhanced visual detection for cavitation of control valve, Chemical *Engineering Research & Design*, 195: 673-681.

[14] Ren, R. Su, T. Ma, F. Wu, X. Xu, C. and Zhao, X. 2022. Study of the influence laws of the flow and cavitation characteristics in an injector control valve, *Energy Science & Engineering,* 10(3): 932-950.

[15] Bianchi, G.M. Falfari, S. Parotto, M. and Osbat, G. 2003. Advanced modeling of common rail injector dynamics and comparison with experiments, *SAE Technical Papers*, 2003-01-0006.

[16] Wang, C. Li, G. Sun, Z. Wang, L. Sun, S. Gu, J. and Wu, X. 2016. Effects of structure parameters on flow and cavitation characteristics within control valve of fuel injector for modern diesel engine, *Energy Conversion and Management*, 124: 104-115.

[17] Kayakol N. 2014. CFD modelling on flow characteristics of two phase flow in solenoid valves, CONV-14 International Symposium on Convective Heat and Mass Transfer, Kusadasi, Turkey.

[18] Zhao, J. Chen, S. Yang, G. and Zhang, H. 2024. Simulation study on the cavitation distribution in the ball valve of a common rail injector, *International Journal of Engine Research*, 25(8): 1575-1587.

[19] Miao, X. Chang, A.B. Zheng, J. Chen, X. Guo, L. Xia, S. Zhou, J. Wang, C. Zhao, Z. Xing, F. and Di, Y. 2024. Flow analysis of a control ball valve in a common rail fuel injector, *International Journal of Engine Research*, 25(5): 1013-1023.

[20] Ko, S. and Song, S. 2015. Effects of design parameters on cavitation in a solenoid valve for an electric vehicle braking system and design optimization, *Journal of Mechanical Science and Technology*, 29(11): 4757-4765.

[21] Ndiaye, E.H.I. Bazile, J.P. Nasri, D. Boned, C. and Daridon, J.L. 2012. High pressure thermophysical characterization of fuel used for testing and calibrating diesel injection systems, *Fuel*, 98: 288-294.

[22] Zhao, J. Liu, W. Zhao J. and Grekhov, L. 2020. Numerical investigation of gas/liquid two-phase flow in nozzle holes considering the fuel compressibility, *International Journal of Heat and Mass Transfer*, 147:118991.

[23] Salvador, F.J. Jaramillo, D. Romero, J.V. and Roselló, M.D. 2017. Using a homogeneous equilibrium model for the study of the inner nozzle flow and cavitation pattern in convergent-divergent nozzles of diesel injectors, *Journal of Computational and Applied Mathematics*, 309: 630-641.

[24] Abdol-Hamid, K.S. Pao, S.P. Massey, S.J. and Elmiligui, A. 2004. Temperature corrected turbulence model for high temperature jet flow, *Journal of Fluids Engineering,* 126(5): 844-850.

[25] Saha, K. Abu-Ramadan, E. and Li, X. 2013. Modified single-fluid cavitation model for pure diesel and biodiesel fuels in direct injection fuel injectors, *Journal of Engineering for Gas Turbines and Power*, 135(6): 1-8.

[26] Yakhot, V. and Orszag, S.A. 1986. Renormalization group analysis of turbulence. I. Basic theory, *Journal of Scientific Computing*, 1(1): 3-51.

[27] Singhal, A.K. Athavale, M.M. Li, H. and Jiang, Y. 2002. Mathematical basis and validation of the full cavitation model, *Journal of Fluids Engineering*, 124(3): 617-624.

[28] Singhal, A.K. Vaidya, N. and Leonard, A.D. 1997. Multi-dimensional simulation of cavitating flows using a PDF model for phase change, *ASME Fluids Engineering Division Summer Meeting*, Vancouver, Canada.

[29] Zwart, P.J. Gerber, A.G. and Belamri, T. 2004. A two-phase flow model for predicting cavitation dynamics, *5th International Conference on Multiphase Flow*, Yokohama, Japan.

[30] Schnerr, G.H. and Sauer, J. 2001. Physical and numerical modeling of unsteady cavitation dynamics, *4th International Conference on Multiphase Flow*, New Orleans, USA.

[31] Jablonská, J. 2013. Modelling on cavitation in a diffuser with vortex generator, *EPJ Web of Conferences*, 45: 01045.

[32] Sa, B. Klyus, O. Markov, V. and Kamaltdinov, V. 2021. A numerical study of the effect of spiral counter grooves on a needle on flow turbulence in a diesel injector, *Fuel*, 290: 120013.

[33] Ren, R. Su, T. Ma, F. Yang, W. Zhao, X. and Xu, C. 2023. Research on the effect of the outlet throttle diameter deviation on the pressure relief rate of the injector control valve, *Energies*, 16(1): 50.

[34] Liu, J. Liu, Z. Wu, J. and Gu, X. 2022. Numerical study on cavitation flow characteristics in diesel fuel injector control valve, *International Journal of Automotive Technology*, 23(4): 881-897.

[35] Guo, G. He, Z. Wang, Q. Lai, M. Zhong, W. Guan, W. and Wang, J. 2021. Numerical investigation of transient hole-to-hole variation in cavitation regimes inside a multi-hole diesel nozzle, *Fuel*, 287: 119457.

[36] He, Z. Guan, W. Wang, C. Guo, G. Zhang, L. and Gavaises, M. 2022. Assessment of turbulence and cavitation models in prediction of vortex induced cavitating flow in fuel injector nozzles, *International Journal of Multiphase Flow*, 157: 04251.

[37] Chorążewski, M. Dergal, F. Sawaya, T. Mokbel, I. Grolier, J.E. and Jose, J. 2013. Thermophysical properties of Normafluid (ISO 4113) over wide pressure and temperature ranges, *Fuel*, 105: 440-450.

[38] Hult, J. Simmank, P. Matlok, S. Mayer, S. Falgout, and Linne, Z.M. 2016. Interior flow and near-nozzle spray development in a marine-engine diesel fuel injector, *Experiments in Fluids,* 57: 1-19.

9 CONTACT

First Author: Mr. Weilong Liu

College of Power and Energy Engineering, Harbin Engineering University, Harbin, China

Email: dc0423@foxmail.com

Second Author: Mr. Xiang Tan

College of Power and Energy Engineering, Harbin Engineering University, Harbin, China

Email: tanxiang@hrbeu.edu.cn

Third Author: Mr. Yu Xu

College of Power and Energy Engineering, Harbin Engineering University, Harbin, China

Email: axlville@163.com

Forth Author (Corresponding Author): Prof. Jianhui Zhao

College of Power and Energy Engineering, Harbin Engineering University, Harbin, China

Email: zhao163.163@163.com